Investigation of Z_{eff} profiles from visible bremsstrahlung in TJ-II plasma scenarios and its correlation with impurity transport behavior deduced by laser blow-off

B. Lopez-Miranda, A. Baciero, B. Zurro, M. A. Ochando, F. Medina,
I. Pastor and the TJ-II team.

Laboratorio Nacional de Fusión, CIEMAT, Madrid, Spain

INTRODUCTION. The study of impurity behavior in fusion plasmas is of paramount importance for understanding its transport and for reactor performance to achieve fusion research goals. Effective ion charge, Z_{eff}, is one of basic plasma parameters used to estimate impurity content in high-temperature plasmas while impurity profile measurement is essential for studying impurity transport in the plasma core. Whereas in tokamak plasmas several methods are available to estimate the Z_{eff} [1], in stellarator devices, which lack a significant current, only bremsstrahlung measurements in visible and soft X-ray ranges can be used for this purpose. Previous attempts to measure Z_{eff} profiles in TJ-II plasmas by means of visible bremsstrahlung (VB) profiles[2,3] provided unrealistic Z_{eff} values that were much higher than those estimated by soft X-ray measurements, whose emission was modeled with a single impurity. Here the VB approach is modified with two improvements: an upgrading of our spectral system to eliminate some caveats in the measurements and interpretation, plus combined spectral measurements with transport code simulations to provide Z_{eff} profiles for evaluating their consistency. Although, many diagnostic systems[4-6] have been set up in magnetic fusion devices to measured Z_{eff}, very few profiles can be found in the literature, in particular in the low electron density range ($<10^{19}$ m^{-3}) addressed in this work and for high Z_{eff} values reported in another device[7]. Finally, our interest in this measurement stems not only from its sensitivity to plasma contamination by different sources, but also because of its sensitivity to impurity transport coefficients that could provide a complementary means to constrain and compare the latter with those determined by other methods.

EXPERIMENTAL AND DATA ANALYSIS. The experiment reported here was performed in the TJ-II: a four-period, low magnetic shear stellarator with major and average minor radii of 1.5 m and ≤0.22 m, respectively[8]. During the Neutral Beam Injection (NBI) heating phase, higher and more peaked electron densities (line-averaged density, $\bar{n}_e \leq 6\times10^{19}$ m^{-3}) are achieved than in the Electron Cyclotron Resonance Heating (ECRH) phase. Moreover the electron temperature profiles are flat with core values in the range 0.3 to 0.35 keV. The

experimental set-up and plasma observation geometry, previously reported in Ref. [2], has been upgraded in two points: A Charge-Coupled Device (CCD) camera has been attached to the second spectrometer focal plane, whilst in the other one a photomultiplier (PMT) is located. Also, a low-resolution spectrometer covering the entire spectral range of interest from 200 to 900 nm has been added to study the real dependence of VB emission with wavelength and in this way being able of separating other mechanisms producing continuum radiation in the visible and near UV range. By changing the mirror that selects the operational focal plane, a survey can be made, prior to performing any VB profile measurement, to identify the emission lines present in the spectral range used to scan the VB. The main advantages this approach are: 1) different spectral ranges, free from line emissions, can be identified and explored in order to check the true origin of the detected VB radiation; 2) the spectral range width can be easily tuned by varying the grating type; 3) only a single detector and its electronics are required. As in the previous work[2], system calibration was performed using measurements from a low-radiation level discharge, in which the Z_{eff} was assumed to be close to 1. Then, starting with an emission profile calculated for $Z_{eff} = 1$, its profile is modified during an iterative process until a match with the experimental chord-integrated emission profile is obtained. Note: it has been determined that the Z_{eff} from one half of the profile does not describe the complete emission profile. This may indicate the presence of other effects that are not considered in the model, *e.g.*, profile asymmetries or reflections off the vacuum vessel. Nevertheless these profiles can be compared with those calculated with the STRAHL code[9] by assuming that local profiles are symmetric. For chord-integrated plasma the relationship between measurement time and spatial position is needed. The various steps needed are described in Ref. 2. Finally, a tomographic inversion method, based on minimizing Fisher's inversion, was used for analyzing the data.

Z_{EFF} EVOLUTION DEDUCED FROM VB. VB profiles, free of contamination by spectral lines, have been evaluated for different spectral ranges, from the UV to the Near IR. From these, the Z_{eff} evolution was deduced in order to determine their dependence with wavelength along TJ-II discharges during the 2016 campaign. It was found that spectral ranges around 220, 523 and 715 nm are free of significant line emissions, Figs. 1(a) to (c). The values of Z_{eff} are several times higher than those that would be expected from VB originating from electron-ion (e-i) collisions only. However, other effects could cause enhancement of the VB continuum beyond that predicted by the standard formula[2]. Thus it is necessary to include an enhancement factor α so the results are plotted as $\alpha \cdot Z_{eff}$ product, where this factor considers

all enhancing mechanisms of e-i VB such as collective[10] or non-maxwellianity[11] effects, (these will be further investigated in the future).

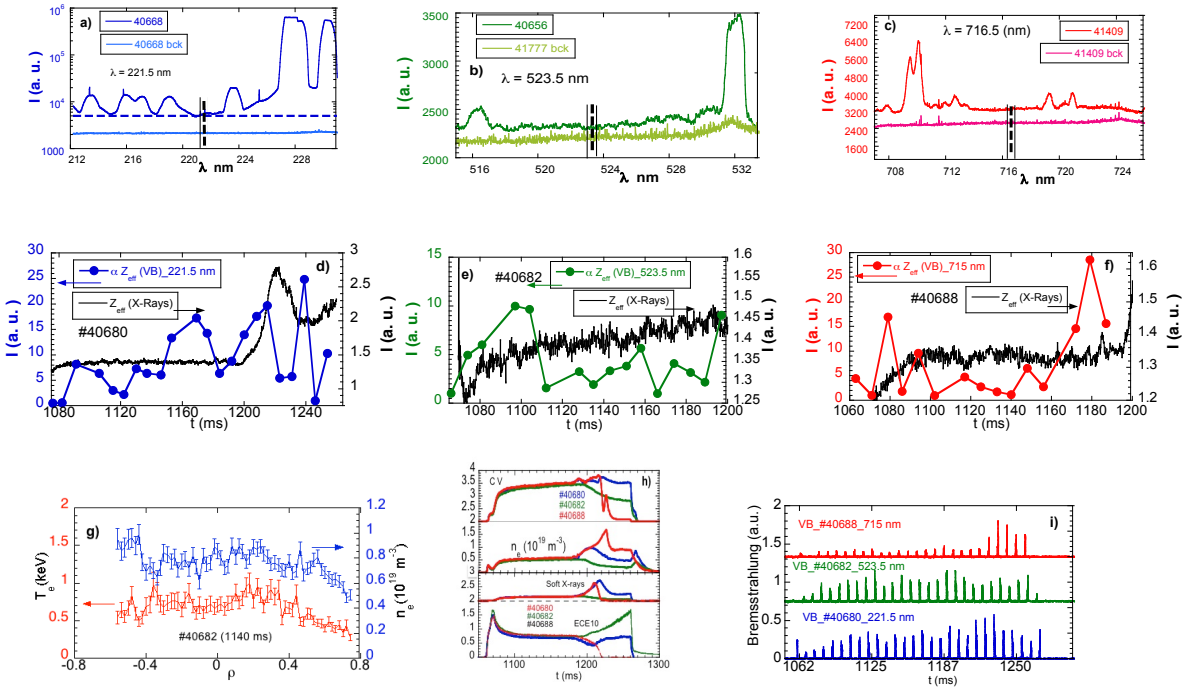

Fig. 1. a) Spectra of free of contamination by spectral lines emissivity for the UV range around 220 nm, b) for the visible range, around 523 nm, and c) for the Near IR, around, 716 nm; d), e) and f), relative evolution along a discharge of $\alpha \cdot Z_{eff}$ for the same spectral ranges; f) Thomson Scattering (TS) profiles of T_e and n_e, g) Time evolution of various signals along three discharges and h) Raw data of the VB profiles used to investigate the Z_{eff} behavior in the plasma interior.

In Figs. 1(d) to (f), the evolution of $\alpha \cdot Z_{eff}$ profiles are plotted at the plasma center, where the n_e and T_e profiles required for their determination are well known, see Fig. 1(g). In contrast, the plasma periphery is not considered due to the large uncertainty in these profiles in the outer regions where, in addition, other mechanisms such as e-n bremsstrahlung[8] or dust effects[12,13] give rise to continuum radiation and thus complicate its interpretation. Typical discharge traces are shown in Figs. 1(h)- (i). A similar analysis has been performed for a discharge with an ECRH phase followed by an NBI phase (see Fig. 2). Here, the higher electron density during the NBI phase also results in high $\alpha \cdot Z_{eff}$ factors, therefore such an enhancement may exist at all plasma densities in TJ-II thus providing a hint as to its origin. To estimate the range of Z_{eff} values consistent with experimental emissivity profile of total radiation in TJ-II, the STRAHL code has be run with two impurities (heavy and light ones) and transport coefficients similar to those estimated from laser blow-off, except for its deposition which is assumed to be at the plasma periphery. We try to investigate their influence in the Z_{eff} value and the relationship with the enhancement factor.

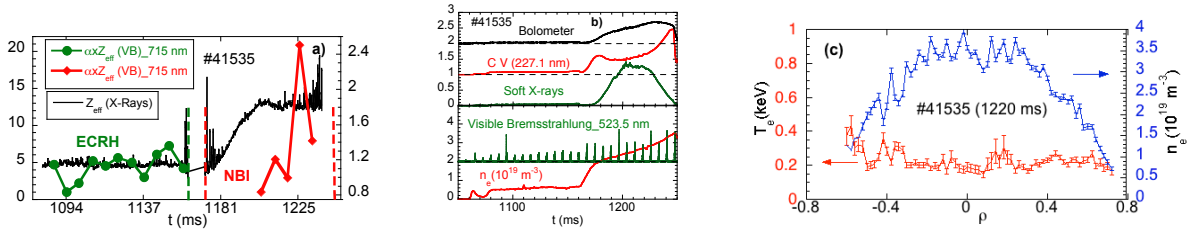

Fig. 2. a) Time evolution of $\alpha \cdot Z_{eff}$, b) time evolution of basic traces and c) TS profiles at 1220 ms for a discharge with ECRH and NBI heating.

We compare bolometric emissivities with those estimated from STRAHL at a given time (22 ms), for specific runs of the code where we try to deduce the closer parameters that give the better fit. In Fig. 3(a) the bolometric radiation profile can be fitted with the combination of tungsten plus boron, W+B, impurities. In Fig. 3(b), the theoretical Z_{eff} deduced for different impurities are compared with those estimated using the VB, the simulated values are close to 1, as it was deduced for X-ray data; while in In Fig. 3(c), showing the temporal evolution of the Z_{eff} profile derived from W+B impurities are compared with those estimated using the VB.

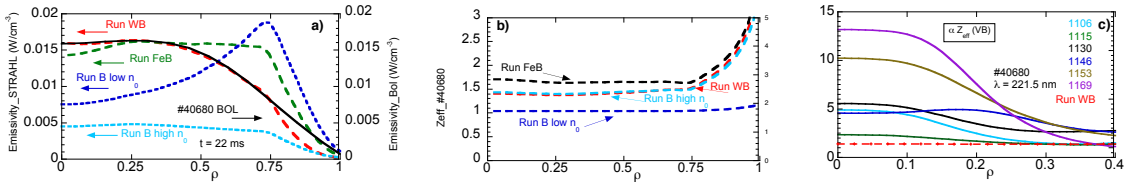

Fig. 3. Comparison of experimental radiation and Z_{eff} profiles with those calculated with the STRAHL code: a) Experimental radiation and STRAHL profiles assuming Fe plus B, W plus B impurities and solely B with a high and low neutral densities; b) The Z_{eff} profiles resulting from the same assumptions as in a) and c) Theoretical and experimental Z_{eff} profiles highlighting the need for an enhancement factor for bremsstrahlung emissivities to account for the differences.

The comparison between experimental and theoretical emissivity profiles for specific runs of the STRAHL returns the best fit when W+B impurities are considered. An enhancement factor has been found developing a careful study of the Z_{eff} evolution at different spectral ranges, which cannot be explained even when a high impurity was introduced into STRAHL.

Acknowledgements. This work was funded by the Spanish "MINECO" under Grant No. ENE2014-56517-R. B.L.M. would like to acknowledge her scholarship, Grant No. BES-2015-075704. The authors are grateful to Drs. E. M. Hollmann and K. J McCarthy for critical reading of the manuscript .

References

[1]Zheng YZ *et al*., 2007 Chinese Physics **16**-1084-1088

[2]Baciero A, Zurro B *et al*., Proc. 30th EPS Conf., St. Petersburg, 7-11 July 2003 ECA **27**A, P-2.80

[3]Baciero A, Zurro B *et al*., Proc. 34th EPS Conf., Warsaw, 2- 6 July 2007 ECA **31**F, P-5.089

[4]Morita S *et al*., 1991 Report ORNL/TM-**11737**

[5]Morita S and Baldzuhn J, 1994 Report IPP III/**199**

[6]Zhou HY, Morita S *et al*., 2010 J. Appl. Phys. **107**, 053306

[7]Anderson JK *et al*., 2003 Rev. Sci. Instrum. 74 2107-2110

[8]Sánchez J, Tabarés F, Tafalla D *et al*., 2009 J. Nucl. Materials **390** 852

[9]Dux R *et a*.,*l* 1999 Nucl. Fusion **39** 111509–22

[10]Tsytovich VN 1995 Phys. Usp. **38** 87–108

[11]Dudík J *et al*., 2012 A&A **539** A107

[12]de la Cal E *et al*., 2013 Plasma Phys. Control. Fusion **55** 065001

[13]Seo-Hee Kim and Young-Dae Jung, 2009 Z. Naturforsch. **64a**, 229 – 232